METAL-ASSISTED CHEMICAL ETCHING OF 4H SILICON CARBIDE

BY

JULIAN MICHAELS

THESIS

Submitted in partial fulfillment of the requirements
for the degree of Master of Science in Electrical and Computer Engineering
in the Graduate College of the
University of Illinois at Urbana-Champaign, 2020

Urbana, Illinois

Adviser:

Professor Xiuling Li

Abstract

Metal-assisted chemical etching (MacEtch) is a wet etching method that can produce high aspect ratio nanostructures with minimal crystal damage. The MacEtch process has been demonstrated to overcome limitations of dry and wet etching in several materials, studied extensively since its discovery by Li and Bohn in 2000. These include several semiconductor substrates (Si, GaAs, InP, GaP, GaN, Ga_2O_3, and SiC) and catalysts (Au, Ag, Pt, Pd, graphene, Cu), each demonstrated with different degrees of anisotropy, porosity, and etching conditions.

SiC has only ever been demonstrated to etch with a porous layer generated using a wet etching method. This is a serious limitation for its applicability to a wider range of etching applications. In this thesis, nanoscale nonporous wet etching is demonstrated on 4H-SiC. Both photolithography and nanosphere lithography are used to pattern the substrate, being compared in etch quality and characteristics. Control of porosity and etch rate are presented, with a mechanism analysis provided to complement the explanations in the literature.

To my brother, Theodore

Acknowledgments

I would first like to acknowledge Professor Xiuling Li for guiding me in my research. She helped me in every step and greatly contributed to my maturation as a researcher.

I would also like to acknowledge Dane Sievers. He aided in experiment design and troubleshooting, metrology, and characterization

Finally, I would like to thank the former and current graduate students in Professor Li's research group, specifically Paul Froeter, Clarence Chan, Hsien-Chih Huang, Lukas Janavicius and Shunya Namiki for their helpful critiques and collaboration.

Contents

1. Introduction

Silicon carbide (SiC) is a wide band gap material that has great promise in a variety of fields. It is currently used in industrial, high-temperature, high-stress applications, and is sometimes considered inimitable in power electronics[1]. SiC is also being developed as a harsh-environment MEMS platform[2], in optoelectronics[3–5], and as a defect-based device platform[6–9]. Etching silicon carbide is difficult due to its being nearly chemically inert, and is usually done with a dry etching process, which is ideal for its current industrial applications that are large in feature size; however, this etching technique is not optimal for nanoscale features, especially those dealing with individual defects. All previously investigated wet etching techniques, the alternatives to dry etching, produce a porous surface, making them all but inadequate for most etching needs, with the exception of producing a porous surface, of course.

The metal-assisted chemical etch (MacEtch) process is a wet etching method that can produce high aspect ratio structures with minimal crystal damage and is herein presented as an alternative to dry etching for nanoscale structures. The thesis is organized as follows. Chapter 1 reviews a variety of SiC applications and etching needs are noted therein. The chapter continues with a review of prominent SiC etch methods, specifically dry etching, electrochemical etching, and MacEtch. The established MacEtch mechanism is reviewed in depth. Results are presented in Chapter 3, beginning with a first principles doping dependence study, followed by initial demonstrated etching. A variety of etching results are presented, patterned with nanosphere lithography (NSL) and photolithography. A study of reagent and pattern dependence is presented for better insight into the etch mechanism, which is subsequently analyzed in Chapter 4. Finally,

results are reviewed and contextualized into the general SiC etching field. Chapter 5 offers a conclusion and overview of propitious further work and projected developments.

2. Literature Review

This chapter will provide a literature review for areas pertinent to the research presented in this thesis. First, SiC applications will be overviewed in Section 2.1, including power electronics, harsh-environment MEMS, optoelectronics, and defect-based quantum devices. An overview of etching techniques is presented subsequently in Section 2.2, focusing on dry etching (subsection 2.2.1), electrochemical etching (subsection 2.2.2) and metal-assisted chemical etching (subsection 2.2.3).

2.1 Silicon Carbide Applications

SiC has several properties that make it a good candidate for a variety of applications. Specifically, the 4H-SiC polytype has a wide band gap of 3.26 eV[10], electron and hole mobilities of 880 and 117 $cm^2\ V^{-1}\ s^{-1}$ respectively[11], and a thermal conductivity of 3.7 $W\ cm^{-1}\ K^{-1}$ [12]. SiC is also one of the toughest semiconductor materials, with a Mohs hardness of 9.5 and near chemical inertness[13]. Due to these characteristics, especially its wide band gap and superb thermal conductivity, SiC is often considered the preeminent semiconductor material for high stress, temperature and power electronics[1]. Many industrial and consumer power electronics utilize SiC; in fact, SiC is beginning to overtake Si as the choice for power MOSFETs in all applications except upon those which lives depend[13].

SiC is also being developed as a material for defect-based quantum devices because of its range of possible intentional defects, which have electrical properties that are comparable to those found in nitrogen vacancies in diamond. SiC has been demonstrated to have coherence times comparable to those found in the nitrogen vacancy centers in diamond[14], to be viable single photon generators[9] (with similar performance as those demonstrated with diamond[15]), and to be a valid

platform for spintronics[16] and potentially quantum computing[6]. Compared to diamond, however, SiC has the distinct advantage of scalability, with mature 6-inch wafer scale production. Patterning SiC is standardized, and for that reason, additional photoluminescent enhancement (outside of the usual cryogenic techniques) has been demonstrated due to localized enhancement[17]. For that reason it is worthwhile to investigate precision nanoscale etching for SiC.

2.2 Silicon Carbide Etching Techniques

With the exception of KOH, SiC is resistant to most chemicals, making it a challenging material to etch. The conventional bulk oxidization and wet etch technique, as used in silicon, is not readily applicable to SiC because of its slow oxidation rate[18]. Though the electrochemical etching of SiC has been studied, the industry choice for etching SiC is plasma-based. The state of the art, specifically the reactive ion etch (RIE), method is reviewed (subsection 2.2.1), followed by the electrochemical etch method (subsection 2.2.2). The final technique reviewed is the metal-assisted chemical etch (MacEtch) method (subsection 2.2.3), whose mechanism will be explained in depth.

2.2.1 Dry Etching

The dry etch process for silicon carbide is the industry standard for all SiC devices because it is the fastest and most reliable etching method. The most rudimentary dry etch uses SF_6/O_2 in an RIE process that leaves no residue[19]. However, the fastest etching of SiC is found in a time multiplexed etch process (TMEP, or Bosch process), whereby inductively coupled SF_6/O_2 plasma is cycled between low and high oxygen content[20]. The Bosch process promotes smoother etching and allows for deeper trenches by limiting etch cutoff with its cycled segments.

While this process is totally sufficient for microscale power electronics, where any crystal damage is too insignificant to tangibly affect device performance, the etch displaces dopants and defects as deep as 190 nm[21]. This degree of damage is acceptable for devices larger than 1 μm, as are most power electronics, but becomes an issue when the device depends on smaller doped areas. The dry etching process is additionally nonideal for nanoscale features as it needs 4% of the final etch depth as a mask, as the metal mask is also attacked by the etch[20,22]. While photoresist can be used as the etch mask, it too must be thick and is only suitable for etch depths up to 0.6 μm[23]. In the standard photolithography patterning process, the resist thickness limits the minimum feature size; the thicker the resist, the larger the smallest feature can be. Moreover, the metal mask must be significantly thicker than the resist for liftoff to be possible. For these reasons, the established dry etching protocol is not ideal for the nanoscale etching of SiC.

2.2.2 Electrochemical Etching

Electrochemical etching of SiC has been explored in literature due to its ability to reliably produce porous SiC, specifically for optoelectronics. The electrochemical etching process involves a wet etch solution containing an electrolyte, an oxide etchant (usually hydrofluoric acid), and water, a metal contacts (usually Pt) that defines the pattern and an ohmic contact (usually on the backside of the sample) across which a voltage is applied[24]. Etching is further enhanced with UV light, which provides additional holes during the oxidation process[25].

Though the process is perhaps the best way to produce porous SiC[26,27], especially for photoluminescent enhancement[28], it is not ideal for smooth etching of SiC as it, as of now, has not been demonstrated to produce nonporous etching. Moreover, electrochemical etching is severely limited in pattern compatibility; all features must be interconnected and have an area large enough

to contact a wire for the induced voltage or must be large enough to be submerged in an agitated electrolytic solution[26].

2.2.3 Metal-assisted Chemical Etching

2.2.3.1 Overview of Etch

First discovered in 2000 by Li and Bohn, metal-assisted chemical etch (MacEtch) is a wet etch process that can produce anisotropic high aspect ratio structures with minimal surface and lattice damage[29,30]. MacEtch has been demonstrated on a variety of materials, including Si[29–34], GaAs[35,36], InP[37,38], β-Ga_2O_3[39], and SiC[28,40,41]. MacEtch can be summarized in two processes: carrier generation and mass transport. Carrier generation begins with a cathodic noble metal or semimetal catalyzing the reduction of oxidants in the reagent solution to produce holes (h^+) that are injected into the valence band of the target semiconductor. The local positive charge attracts oxygen radicals, which are produced during the oxidant reduction, causing local oxidation[33]. The mass transport process proceeds when ionized oxide is removed by an acid (usually HF) during the etching process. The process repeats until reagents are consumed, leaving behind high aspect ratio structures. These two processes are shown for etching Si in Figure 1(a).

For semiconductors with relatively high valence band edges (e.g. Si & GaAs), MacEtch is a forward etch, meaning that the metal sinks on the etch front, due to the ease of hole injection from the catalyst[30,33], as seen in Figure 1(b-d); however several semiconductors, especially those with lower valence band edges, can only be etched inversely with MacEtch (I-MacEtch) due to the limited hole injection to the valence band. In I-MacEtch the metal serves both as a cathode and a mask – it does not sink during the etch[39,42]. The resulting etch depends largely on the material,

often on the crystallographic orientation, varying from near isotropy in one orientation to anisotropy in another[39,42].

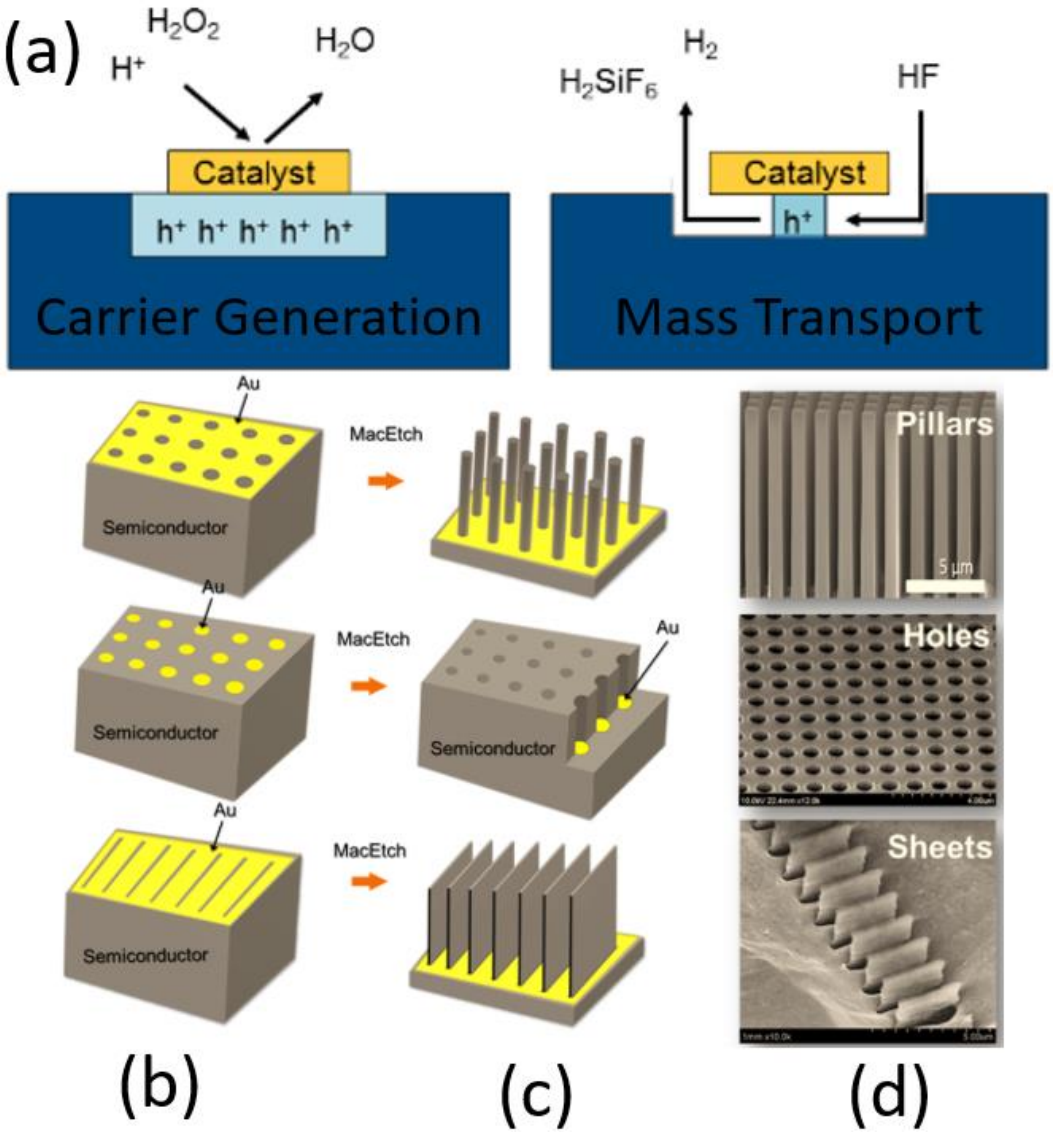

Figure 1: (a) Carrier generation and mass transport processes in the Si MacEtch platform. (b-d) Schematics and SEM images of MacEtch process on Si. (b) Schematic of patterned catalyst and substrate before etching. (c) Schematic of etched substrates. (d) SEM of etched substrates.

2.2.3.2 Review of SiC MacEtch

Due to its lower valence band edge, SiC etches inversely by the established MacEtch methodology. Pt is used as the cathode, HF to remove the oxide, and H_2O_2, $K_2S_2O_8$, and $Na_2S_2O_8$

are used as electrolytes[40,41,43]. Weak hole injection brought about by the low valence band energy is supplemented with above-band-gap UV light (254 nm). Though the exact chemical reaction and physical mechanism are not fully understood (and to that end, not apodictically confirmed through experimentation or theoretical application for any MacEtch process), the reaction is often summarized with three essential steps: electron consumption (1), oxidation (2), and oxide removal (3).

$$4S_2O_8^{2-} + 8e^- \xrightarrow{UV} 8SO_4^{2-} \quad (1)$$

$$SiC + 4H_2O + 8h^+ \xrightarrow{UV} SiO_2 + 8H^+ + CO_2 \quad (2)$$

$$SiO_2 + 6HF \rightarrow H_2SiF_6 + 2H_2O \quad (3)$$

The chemical equations above are balanced and account for the generation and removal of oxide at the surface; however, all published MacEtch processes on SiC generate a porous layer, which is not adequately explained by this chemical mechanism. This thesis includes examples of nonporous etching (Chapter 3) and a discussion of the mechanism, and presents two explanations for the formation of the porous layer.

3. Description of Research Results

This chapter describes all experimental research and demonstrations in this study. Given the goal of this project to produce high aspect ratio nonporous nanoscale selective etching, the study began with a pursuit of any etch that produced defined features. This result was not demonstrated early. Section 3.1 shows all experiments done prior to the achievement of controllable etching, specifically the minimal etching on undoped SiC (subsection 3.1.1), a doping dependence study (subsection 3.1.2), and the initial etching demonstration (subsection 3.1.3). Subsection 3.2 has the true etching results, with the first nonporous NSL etching demonstrated (subsection 3.2.1), a demonstration of porous nanosphere pattern etching (subsection 3.2.2), 5 μm pillars demonstrated (subsection 3.2.3), and a study of the porosity and etch rate based on the Pt pattern and $K_2S_2O_8$ concentration. Smoothing techniques, specifically thermal oxidation (subsection 3.3.1) and ozone treatment (subsection 3.3.2) are discussed in Section 3.3.

Two patterning techniques were used for this study. The first of these is nanosphere lithography (NSL), where nanoscale (or microscale) spheres are dispersed on a substrate and form a periodic array of hexagonally oriented circular patterns. The NSL pattern before etching is displayed in Figure 2(a). The other patterning technique utilized is conventional photolithography, which is used by itself as a mask and also combined with NSL to produce smaller areas of NSL patterning.

A 10 nm Pt mask is used for all etching and was deposited using E-beam evaporation. $K_2S_2O_8$ is used as the electrolyte, and 254 nm, 9 mW/cm^2 UV light is used for carrier generation, unless noted otherwise. Images were taken using scanning electron microscopy (SEM) and cross

sections were obtained with a focused ion beam (FIB). Porosity, measured in surface roughness, was measured using a Keyence VK-X1000 optical profilometer.

3.1 Results Prior to Controllable Etching

Due to problematic substrates, cathode delamination, and weak UV light, the initial results in this experimental work were unsuccessful in their goal; however, their analysis, as will be shown in Chapter 4, yields useful information for characterizing the etch.

3.1.1 Undoped SiC Etch

The first experiment carried out with SiC was using a 1 μm NSL pattern thinned to 500 nm, with a 10 nm Pt mask. The substrate was undoped SiC, which was rough on the surface. The etching solution consisted of 10 mL HF and 18 mM $K_2S_2O_8$, and a <1 mW/cm^2 254 nm UV lamp. Due to a combination of surface roughness and undercut, the latter of which was a result of the former and low doping, etching was limited to a few nanometers before Pt delamination halted the etch. The resulting surface had minor adherence to the pattern with poor etch filling (not all the exposed regions were etched) and very small etch depth, seen in Figure 2.

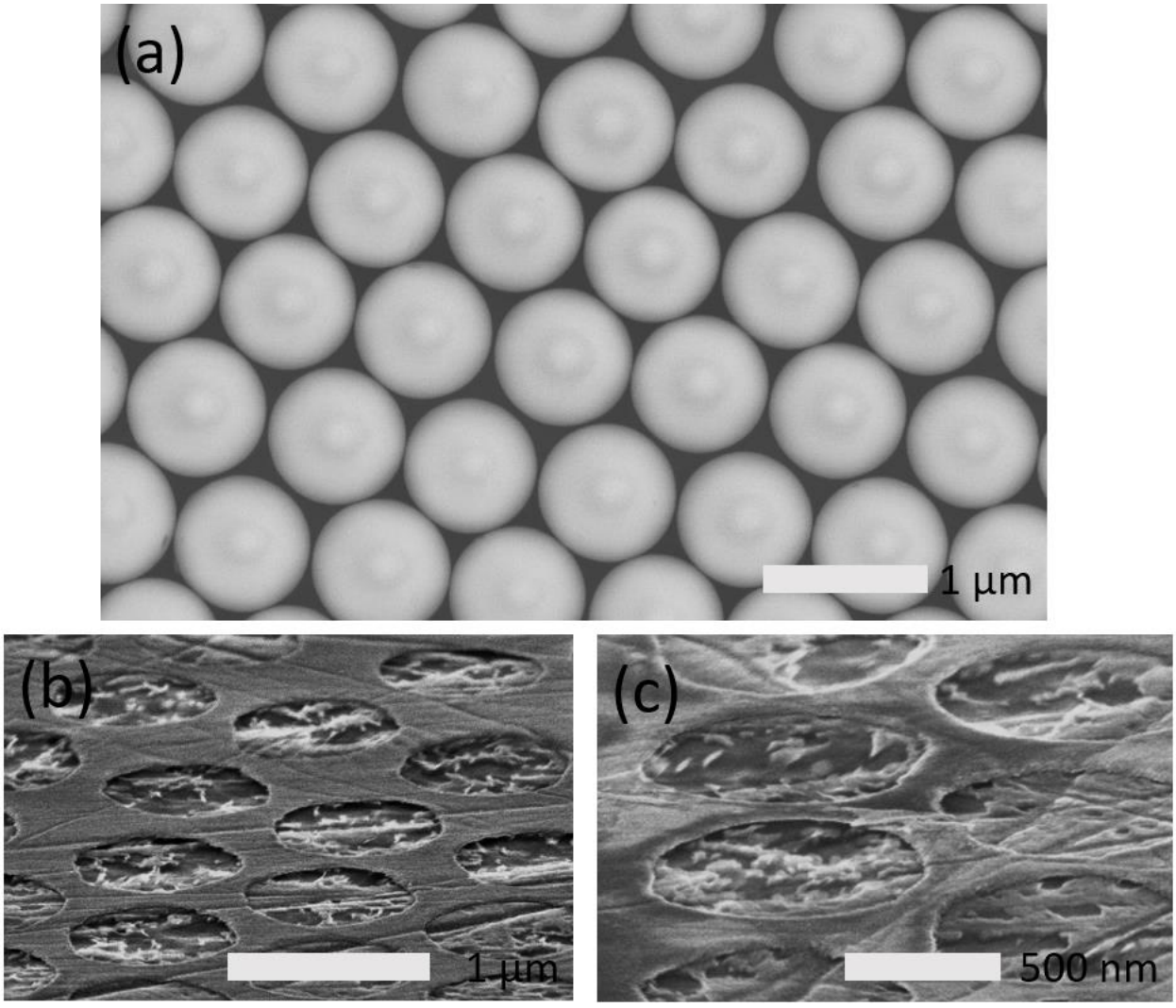

Figure 2: (a) 1 µm NSL pattern before thinning. (b,c) Angled views of etched undoped SiC substrates patterned with NSL technique. The flat layer is PT and the rough areas exposed are the etched SiC.

3.1.2 Doping Dependence Study

The results of the first study made the factor of doping dependence especially pertinent; it was believed at the time that the poor etching was in part due to the low doping, which would imply higher mobility, therefore increased lateral movement of holes, and therefore more undercut, leading to Pt delamination. This experiment took the undoped SiC substrate and thermally doped it with borosilicate wafers in increasing doses. Though the exact doping concentration was not

measured, it could be estimated that one was nearly undoped (~10^{14} cm^{-3}), one moderately doped, and one degenerately doped (~10^{20} cm^{-3}). The sample was sputtered with a noncontinuous 4 nm Pt layer, which appeared as flakes on the surface. Finally, the sample was etched in 10 mL HF, 18 mM $K_2S_2O_8$, and a <1 mW/cm^2 254 nm UV lamp. The resulting etch showed increased etching with increased doping, as seen in Figure 3. Though this study was not quantitative, it demonstrated something not shown in the literature: the MacEtch of SiC is strongly dependent on the doping concentration of the substrate.

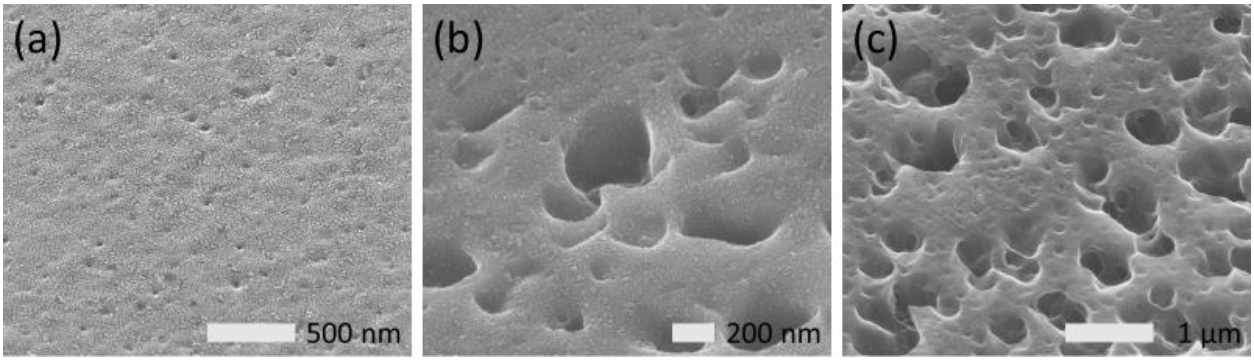

Figure 3: SEM images showing etching porosity by boron doping concentration. Samples were etched for 1 hour with 4 nm noncontinuous Pt (visible as white flecks in the images above). (a) Undoped (1014 cm^{-3}) SiC. (b) Moderately doped SiC. (c) Degenerately doped (~1020 cm^{-3}) SiC.

3.1.3 Initial Etch Demonstration

The first demonstration of truly patterned etching was with a doped sample, ~10^{18} cm^{-3} N (n-type) doped 4H SiC, with a 10 nm Pt NSL mask, etched in 10 mL HF, 40 mM $K_2S_2O_8$, and a <1 mW/cm^2 254 nm UV lamp for 48 hours without the reagents replenished. Due to the continuous etching, the reagents had totally evaporated by the end of the etch, meaning that the "48 hours" timescale was inaccurate; moreover, after rinsing the substrate before imaging, there was no Pt mask visible on the surface, implying prior delamination. That said, the resulting etch showed total pattern transfer, with the NSL etched accurately into the substrate with undercut and Pt delamination. There was some inconsistency across the substrate; some areas etched far smoother

and with more isotropy, as shown in Figure 4(a), than others, that were more porous but etched with better anisotropy, as in Figure 4(b). Later analysis showed that this was the result of loss in liquid and therefore increase in UV light.

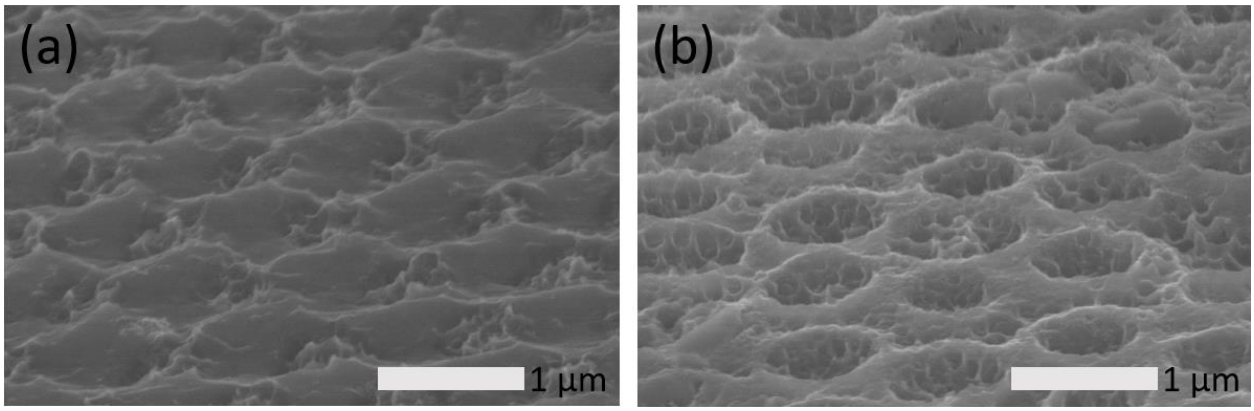

Figure 4: SEM images showing the first successful MacEtch of 4H-SiC using NSL. (a) SEM image showing a nonporous, isotropic etch. (b) SEM image showing a porous but anisotropic etch.

3.2 Etching Results

After the initial successful etch, the following etching was demonstrated. These were all made with a 4H-SiC substrate with the same doping concentration as before. First, a nonporous etching was demonstrated (subsection 3.2.1), achieved with the significant reduction in liquid and with a reduction in the overall amount of Pt on the surface; both of these modifications led to a dramatic increase in UV light penetration, which, as was correctly believed at the time, is the most important variable in this etching process. Next it is demonstrated that the same pattern, NSL, can be etched porously (subsection 3.2.2) by simply changing either the Pt mask coverage or the reactants. The variety of the etch is shown next, with 5 µm wide SiC pillars fabricated (subsection 3.2.3). Finally, the etch dependencies, specifically Pt mask coverage (Area %) and $K_2S_2O_8$ concentration (mM), are studied with respect to etch rate and porosity.

3.2.1 Nonporous NSL Pattern Etching

Nonporous etching of 4H-SiC was first demonstrated with the NSL platform, in a way that mimicked the first successful pattern transfer on the same substrate type. Samples were first patterned with photolithography with a 500 μm wide crosshair pattern, followed by 1 μm NSL patterning, which were smoothed to 500 nm. 10 nm Pt was then deposited using E-beam evaporation, followed by a standard liftoff procedure. Samples were then etched in 6 mL HF and 37 mM $K_2S_2O_8$ for 24 hours, and a 10 mW/cm^2 254 nm UV light with reagents replenished every 4 hours. The resulting etch was anisotropic (undercut of 50%), nonporous, and with vertical sidewalls, displayed in Figure 5(a). Overall, the etch rate was 17 ± 1.4 nm/hr, with a maximum height of a feature at 408 ± 34 nm, as seen in Figure 5(b). The nonporous etching was attributed to the increased UV light incorporated in the reaction, achieved with less liquid reagent (which absorbs the UV light) and less Pt coverage (which, though important in the reaction, also reflects UV light). Some areas, especially those near the border of the crosshair resist, saw less thinning in the NSL pattern, which lead to smaller triangular features with 150 nm sides, shown in Figure 5(c).

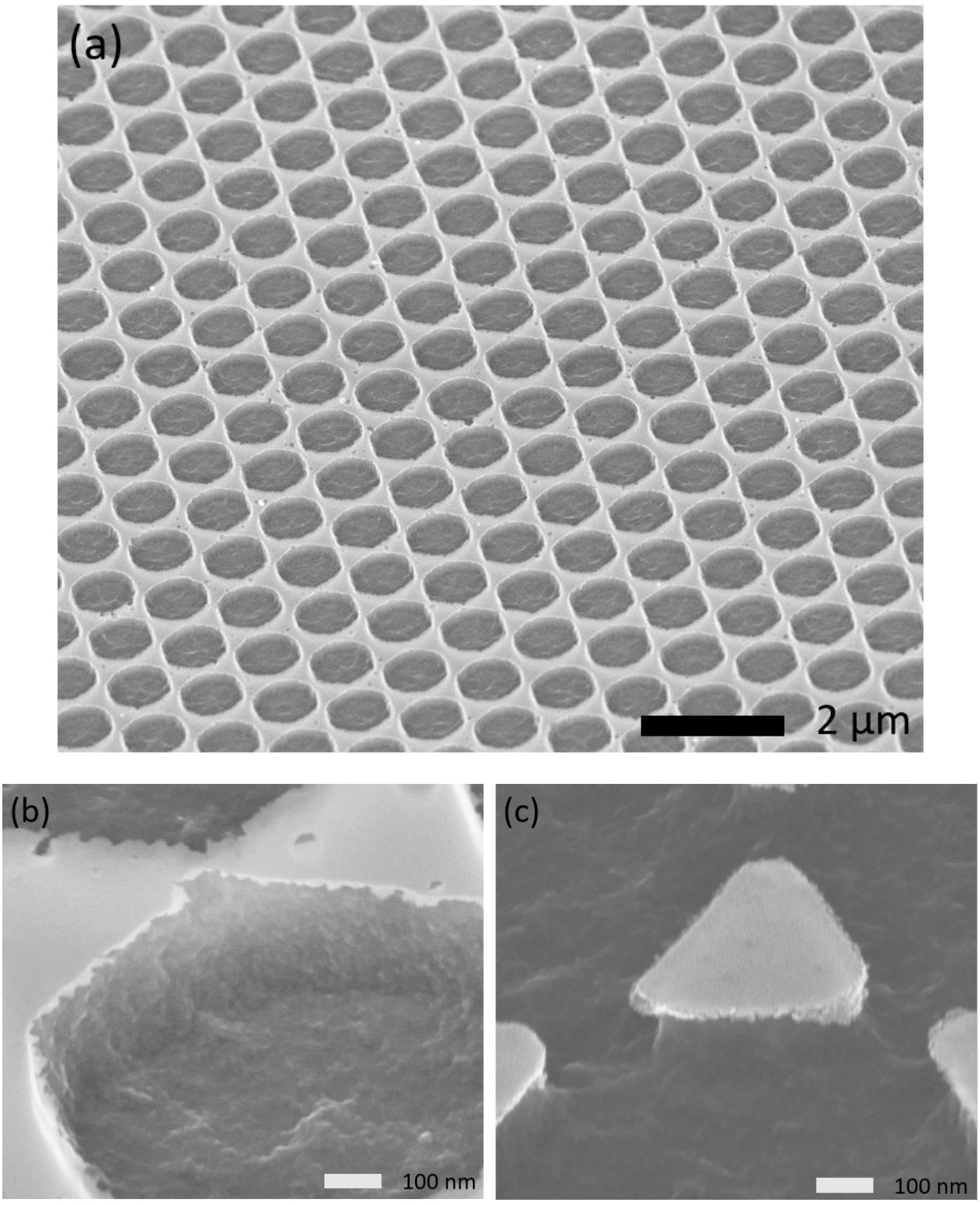

Figure 5: SEM images showing NSL pattern etched SiC. White regions are the remaining Pt mask and the darker gray is the etched SiC. (a) Large area of etched surface. (b) Close-up of etched NSL etched SiC. (c) Close-up of triangular pillars near the border of the resist.

3.2.2 NSL Porous Etching Demonstration

Similar sample preparation was used to demonstrate porous etching with the same pattern. The substrate was prepared with the same NSL pattern without the resist crosshairs, so that the entirety of the surface was covered with the pattern. This caused in a vast decrease in exposed SiC (at least 70%), which led to reduced UV absorption during the etch. The resulting etch, shown in Figure 6, was significantly slower, with an etch rate of merely 9.5 ± 2 nm/hr, and significantly more porous. Undercut too was reduced, perhaps due to the lack of local holes. Because of the pattern's total coverage, roughness could not be measured, but the SEM images show that the surface was very porous, comparable to those results presented in subsection 3.2.3.

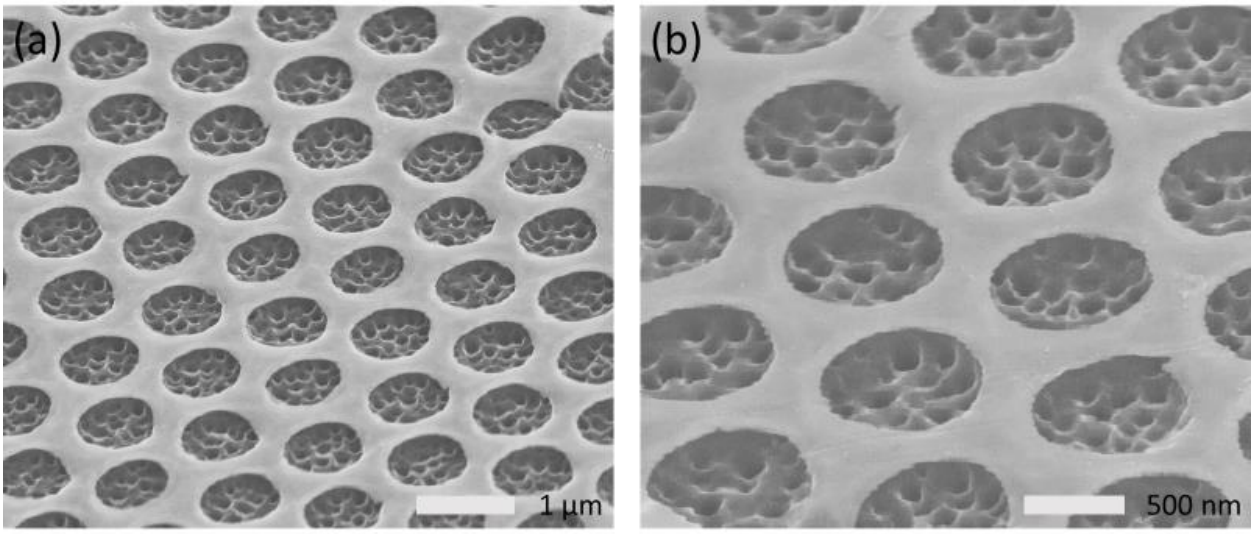

Figure 6: SEM images showing the same NSL pattern with less exposed SiC. Surfaces were significantly more porous, etch rate was reduced, and undercut was minimized. (a) Large area (b) small area of etched surface.

3.2.3 5 µm Pillar Demonstration

To demonstrate etching capability for a more arbitrary pattern, 5 µm circles, spaced 5 µm apart, were used. Again, 10 nm E-beam Pt was used as a mask. The etch included 4 mL HF and 92 mM $K_2S_2O_8$ for 60 hours, with the reagents replenished every 4 hours. The result was highly

porous, with a 62.5° sidewall, with an etch rate of 33 ± 2.3 nm/hour, as shown in Figure 7. This etch demonstrated increased etch rate with more UV availability, with 60% of the SiC area exposed. Additionally, this etch demonstrated the etch was suitable for patterns of isolated features.

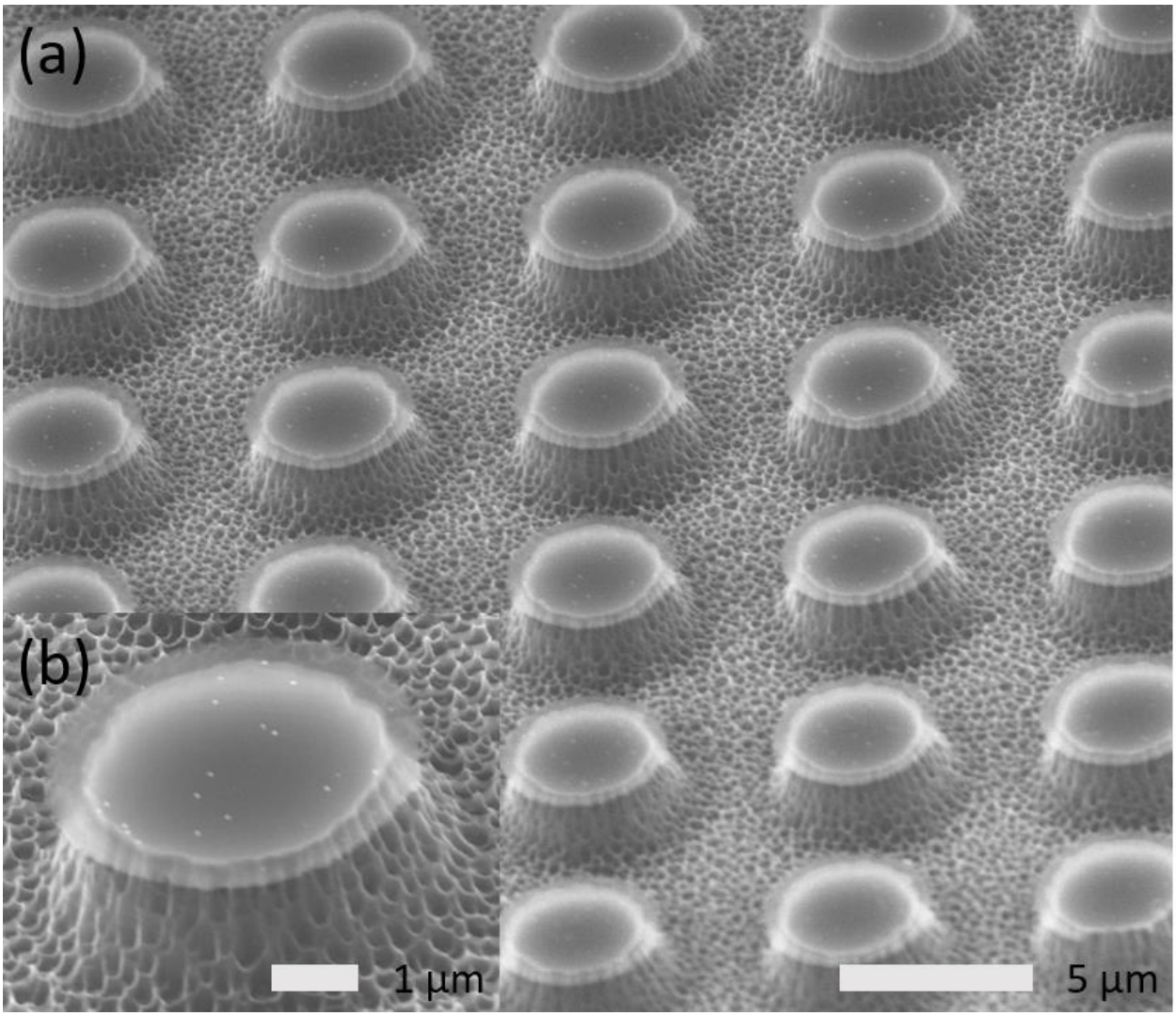

Figure 7: SEM images of the 5 µm pillars. The translucent white disks on top of the pillars are the Pt mask used during etching. Porous etched areas and sidewalls are visible. (a) Wide area view. (b) Close-up view.

Another etch with the same mask and with 111 mM $K_2S_2O_8$ and the same etch conditions above was completed, showing increased porosity and an enhanced etch rate of 68.2 nm/hr. This result showed the dependence of etch rate on the electrolyte concentration.

3.2.4 Porosity Study

A study of the porosity is presented next. Samples of bars with varied spacing and width were fabricated using photolithography and a 10 nm Pt mask. All etches used 4 mL HF, were replenished every 4 hours and went on for a total of 24 hours. $K_2S_2O_8$ concentration was varied, with three samples, etched in 56, 92, and 130 mM $K_2S_2O_8$. The pattern used contained ten regions, each with 500 µm long bars with varying widths and spacings. The resulting etch, with varied porosity, etch rate, and electrolyte concentration, showed a strong dependence of exposed SiC and $K_2S_2O_8$ dependence, displayed in Figure 8(a). Immediately a positive correlative trend can be established with etch rate and electrolyte concentration.

Porosity is not precisely defined, as accurate measurement would require sophisticated tools that are not scalable for a study with this much data, and is instead measured by surface roughness, which although it does not account for the pore depth, gives an accurate reading of the overall porosity; larger pores lead to rougher surfaces and also tend to have deeper porous regions, and smaller pores lead to overall smother surfaces and tend to have shallower porous regions. This was confirmed with focused ion beam (FIB) cross sections of samples with varied etch conditions, shown in Figure 8(b,c). The sample etched in 130 mM $K_2S_2O_8$ solution had a porous layer depth of 350 ± 22 nm, while the sample etched in 92 mM $K_2S_2O_8$ solution had a porous layer depth of 205 ± 19 nm. The sample etched in 56 mM $K_2S_2O_8$ solution was nonporous and therefore its porous layer depth was not measured.

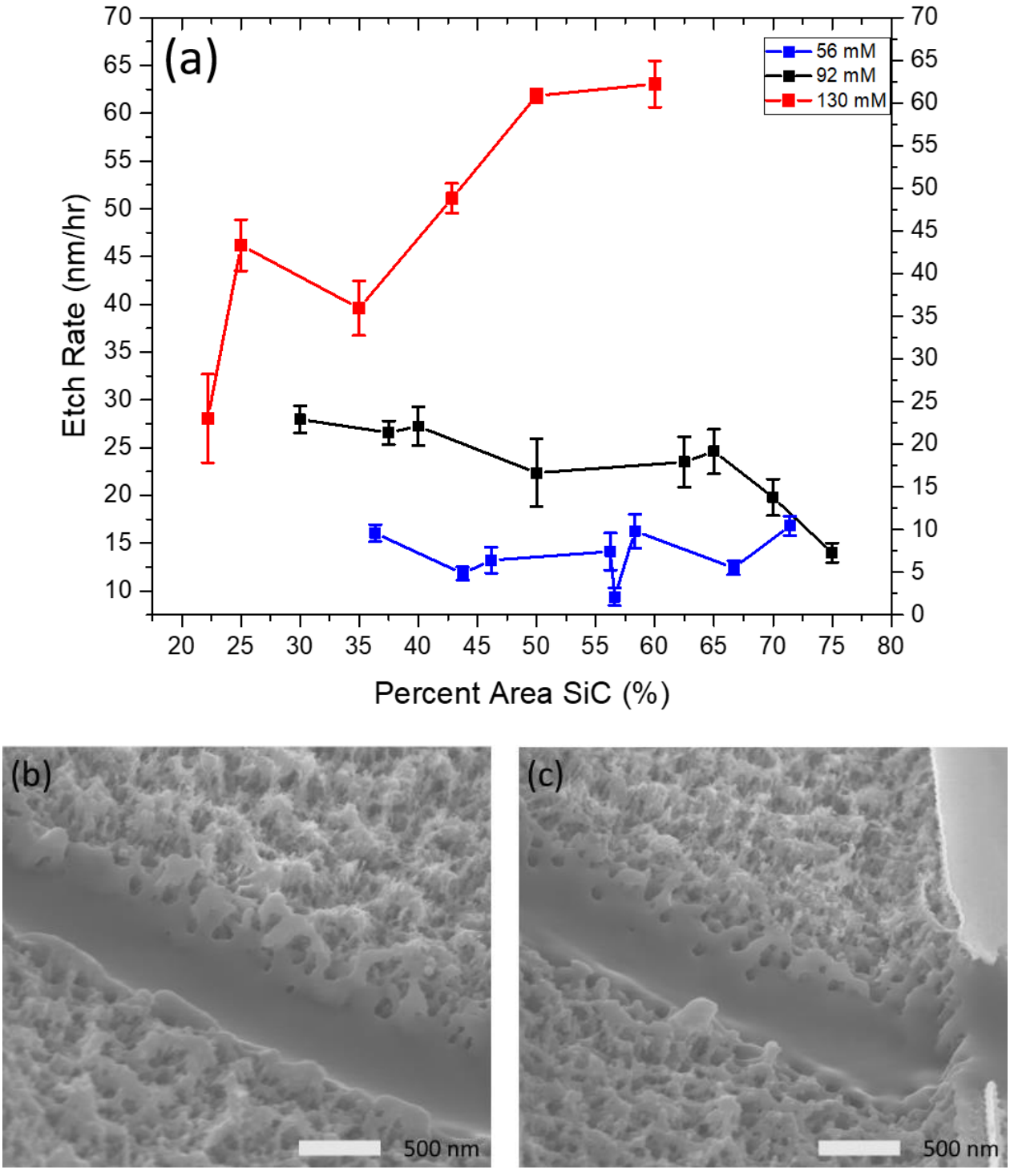

Figure 8: (a) Etch rate by % exposed SiC plotted for three samples, etched in 56 mM $K_2S_2O_8$, 92 mM $K_2S_2O_8$, and 130 mM $K_2S_2O_8$. Some areas delaminated in the etch and were therefore discarded for reporting data. (b,c) FIB cross sectional images of the porous layer for the 130 mM $K_2S_2O_8$ etched sample, each with 350 ± 22 nm depth.

3.3 Smoothing

Because of the porous (or at best nonporous but not smooth) nature of the etch, smoothing techniques were explored. The two smoothing techniques explored in this thesis involve generating an oxide on the substrate surface, removing that oxide, and repeating several times until the desired effects are achieved.

3.3.1 Thermal Oxidation

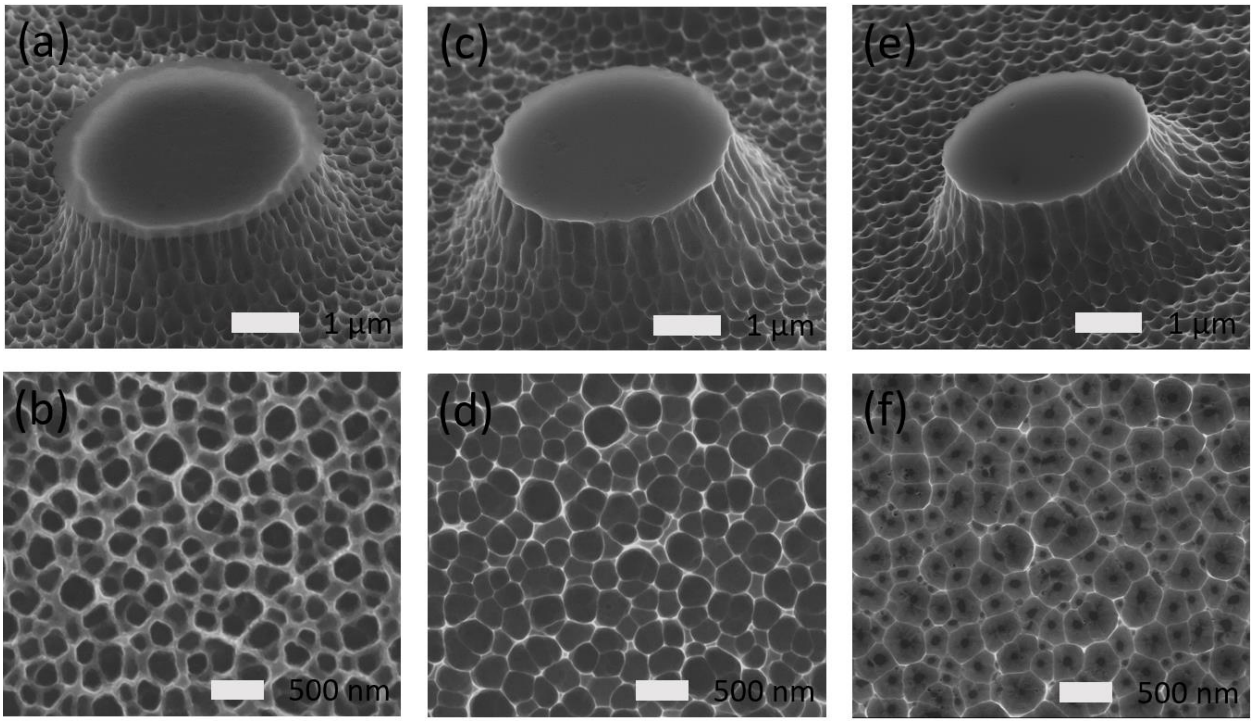

Figure 9: 5 µm pillars before and after smoothing. (a) A pillar after etching. (b) Top-down view of the corresponding porous region. (c) The same pillar after oxidizing 20 nm and etching. (d) Top-down view of the corresponding porous region. (e) The same pillar after oxidizing 35 nm and etching. (f) Top-down view of corresponding porous region.

The simplest method of smoothing the surface is thermal oxidation; however, due to the incredibly slow oxidation rate of SiC, this is not the most practical when removing a porous layer. That said, as outlined in Section 4.4, SiC oxidizes similarly to Si, leaving behind a single layer of insoluble complex oxide ($Si_4C_4O_4$ and $Si_4C_{4-x}O_2$) layer[44]. A 5 µm pillar sample, which was etched

in 92 mM $K_2S_2O_8$, was used to test the efficacy of this technique. The sample was exposed to steam oxidation (110 sccm O_2, 40 sccm H_2) for varying amounts of time, grew an oxide layer, and then etched in 50:1 H_2O:HF solution to remove the oxide. Figure 9 shows the porous surface (a,b) before smoothing, (c,d) after 60 mins of oxidation (20 nm SiC removed) and (e,f) after 90 mins of oxidation (separately, 35 nm SiC removed). The figure is not entirely clear because of the relatively small visual difference; however, smoothing decreased the surface roughness to 73 ± 3 nm and 60 ± 7 nm respectively, from the starting value of 89 ± 9 nm, implying a significant decrease in surface roughness and therefore porosity after a short oxidation treatment.

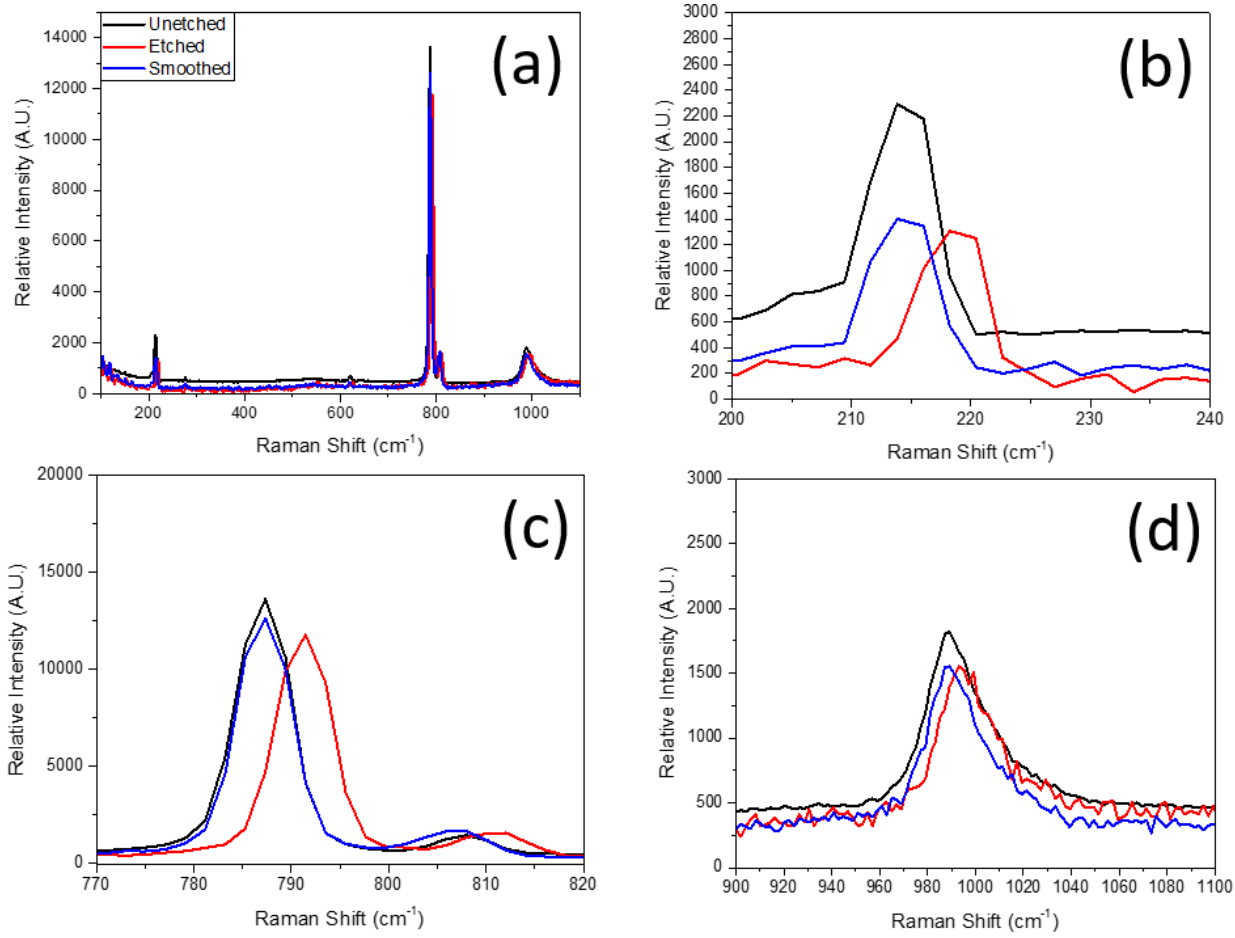

Figure 10: Raman spectra of bare, etched, and smoothed 4H-SiC substrates. (a) Entire Raman spectrum. (b) E2 TA peak, (c) E1 peak, and (d) A1 LO peak, all exhibiting shifts after etching that are removed after smoothing indicating surface states generated by the porous layer.

A brief additional study of the effect of porosity and smoothing was completed by taking Raman spectra of the unsmoothed and smoothed (35 nm SiC removed) sample, in addition to a bare SiC substrate. The etched sample showed significant shifting in all peaks, especially those corresponding to the E_2 transverse acoustic (TA), E_1, and A_1 longitudinal optic (LO) phonons, implying surface states forming caused by the porous layer[45]. After smoothing, however, this shift all but disappeared, and was within a margin of error of the unetched SiC substrate. The Raman spectra for this experiment are displayed in Figure 10.

3.3.2 Ozone Treatment

Ozone (O_3) is a far more efficient method of oxidizing SiC that does not require any heating and therefore is much more time economical, and dopant and intentional defect friendly. The O_3 is simply generated by a UV light in presence of O_2 and that O_3 reacts directly with the SiC surface. Though O_3 only oxidizes the first few layers of material, it is more effective at doing so; moreover, the "first layer" may penetrate down several hundreds of nanometers, because of the porous layer that is intended for removal. It is for this reason that, after only 15 minutes of effective treatment (3 rounds of 5 mins O_3 exposure, 5:1 HF:H_2O), more surface smoothing is observed, as seen in Figure 11(c,d), compared to the original porous surface, Figure 11(a,b).

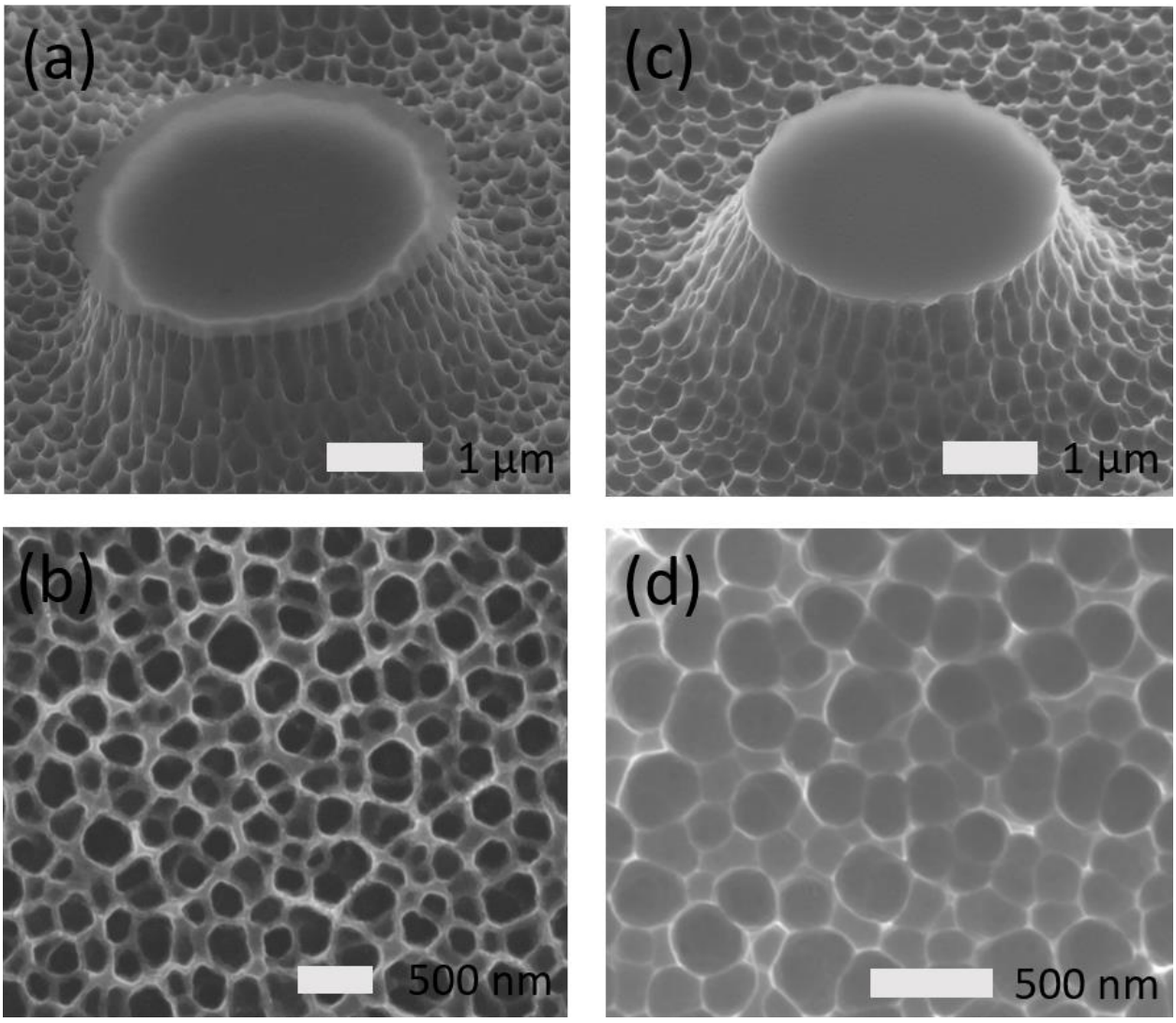

Figure 11: 5 µm pillars before and after smoothing. (a) A pillar after etching. (b) Top-down view of the corresponding porous region. (c) The same pillar after O3 treatment and etching. (d) Top-down view of the corresponding porous region.

4. Analysis of Results

This chapter aims to analyze the results presented in the preceding chapter and contextualize them with other research. Section 4.1 overviews the results, focusing on their broad impact. Sections 4.2 and 4.3 discuss the dependence of doping and UV light in the MacEtch process respectively, revisiting the contributions from the research community (first discussed in 2.2.3.2) and parsing the results herein. Finally, Section 4.4 analyzes the MacEtch mechanism, again revisiting the research community's proposed (but unconfirmed) mechanism and scrutinizing it, adjusting it to fit experimental results.

4.1 Overview of Results

The main result of this thesis is nonporous wet etching of SiC, not yet achieved with any other method. This result singles out MacEtch as the one wet etch method that can etch SiC without forming a porous layer. Preliminary results show an etch tunability in rate, porosity, and undercut based on Pt pattern, UV intensity, and electrolyte concentration. That said, more work must be done to perfect the etching characteristics to make the etch more comparable to industrial dry etching for large features. The present etch is optimized for nanoscale etching, with features as small as 150 nm demonstrated, achievable only because the MacEtch process requires the same height of metal for all depths. While metal height is not a factor for the majority of SiC etching, it plays a significant role in precision details and especially in small patterns; the mask metal must be significantly smaller than the resist used to pattern the features.

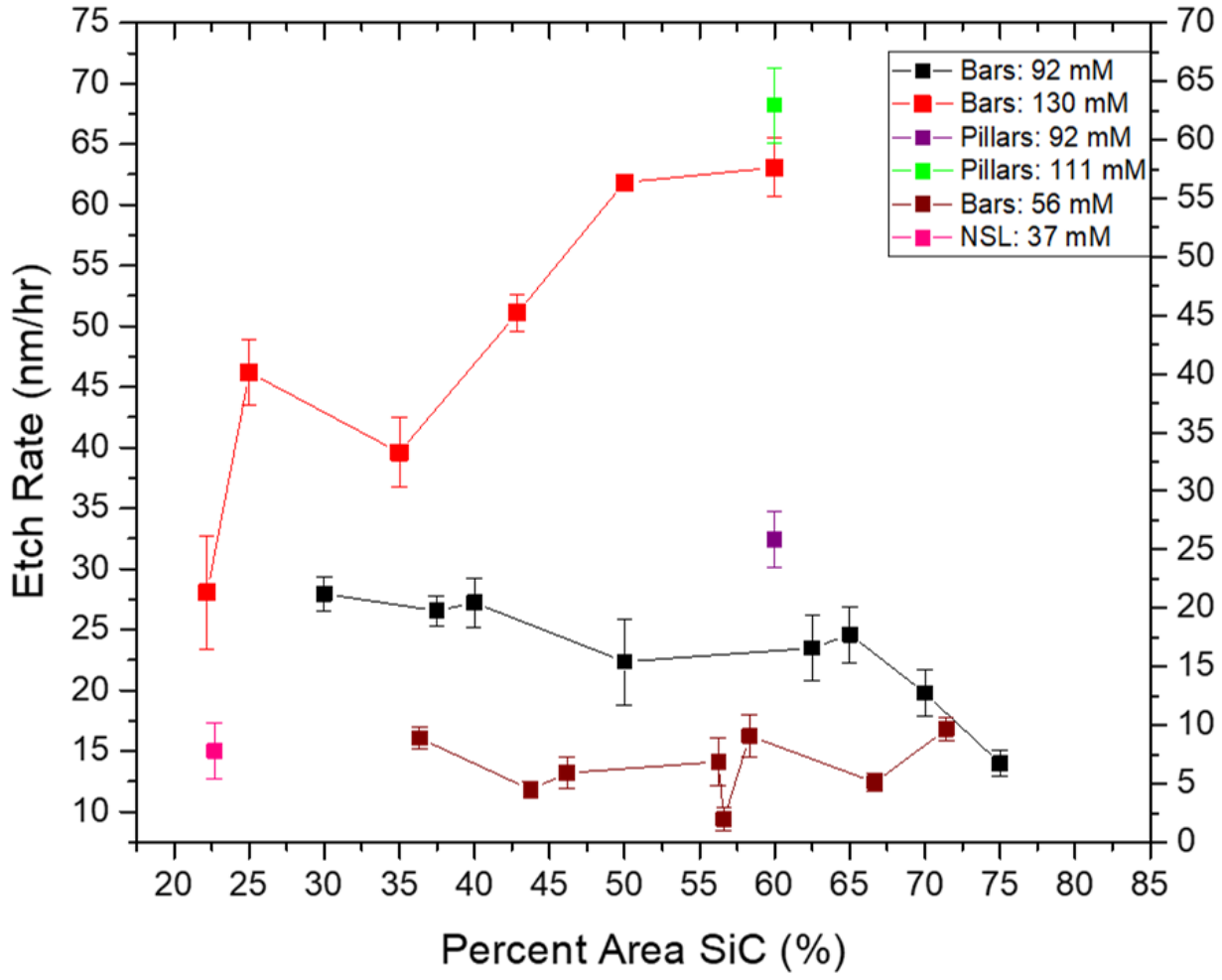

Figure 12: Plot of etch rate vs. percent area SiC for several etched samples.

The experiments reviewed all had similar conditions: the same metal, the same reagents, and the same wafer (with one exception). Only UV intensity, Pt pattern (which defines the features), and electrolyte concentration are systematically studied; however, these two variables are shown to have crucial influence on the resulting etch.

4.2 Discussion of UV, Pattern, and Dopant Dependence

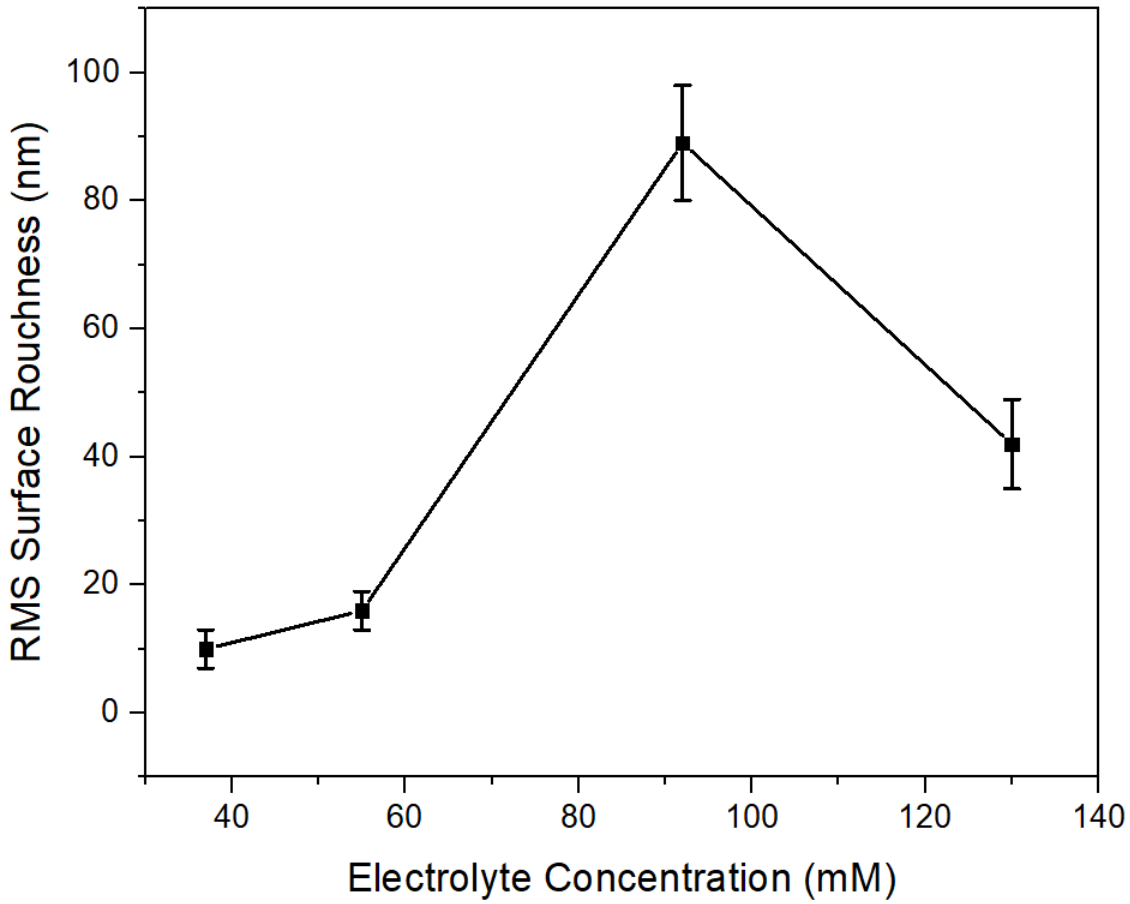

Figure 13: Plot of RMS surface roughness (correlated to porosity) by electrolyte ($K_2S_2O_8$) concentration.

Figure 12 shows the etch rate dependence on Pt pattern (in % Pt coverage) and electrolyte concentration for all samples, combining both the results presented in subsection 3.2.4 and the other etched samples. Some NSL samples could not be measured due to their exceedingly small feature size and were thusly not included in the figure. There is an undeniable trend of increased etch rate with small Pt patterns (corresponding to more exposed SiC), without an indication of a limit; that said, control experiments (not explored herein) demonstrate that Pt is needed for the etch to occur.

Porosity appears to depend not on the pattern, but only on electrolyte concentration and UV intensity. The resulting surface roughness values are plotted by $K_2S_2O_8$ concentration in Figure 13. It appears from the trend that porosity is minimized when $K_2S_2O_8$ concentration is maximized, which causes the index of refraction of the etching solution to increase, thereby blocking UV, and minimized when $K_2S_2O_8$ concentration is minimized, thereby allowing maximum UV light to penetrate. Though it may seem obvious to remove the $K_2S_2O_8$ altogether to promote smoother etching, it must be kept in mind that the etch slows to a halt without it, as can be inferred with the data in Figure 12.

4.3 Discussion of Etching Mechanism

The mechanism of metal-assisted photochemical etching of silicon carbide proposed in literature insufficiently describes the experimental results; specifically, it does not explain the formation of a porous layer during etching. The described mechanism claims that that holes are generated solely at the cathode by the dissociation of the persulfate radical:

$$4S_2O_8^{2-} + h\nu \rightarrow 8SO_4^{2-} + 8h^+ \quad (4)$$

This is followed by local oxidation of the silicon carbide surface, finished with the removal of the formed oxide:

$$SiC + 4H_2O + 8h^+ \rightarrow SiO_2(s) + 8H^+ + CO_2(g) \quad (5)$$

$$SiO_2 + 6HF \rightarrow H_2SiF_6 + 2H_2O \quad (6)$$

While the mechanism in the literature is fully balanced and accounts for all chemicals, it does not provide an explanation for the formation of the porous layer prevalent in all the results; moreover, counter to the experimental evidence, it predicts strong etch preference to areas directly

around the cathode because of the localized hole generation. The first remedy was proposed by Leitgeb et al.[46], where it was claimed that hole generation cannot occur entirely at the cathode – otherwise, the etch would be entirely dependent on the distance from the cathode. Leitgeb demonstrated that it, in the case of focused UV light, etch depends on distance from UV light very strongly but not at all on distance from the Pt contact (cathode). However, hole generation at the cathode explains undercut in the etch, which should not occur if hole generation is confined to areas exposed to UV. Moreover, Leitgeb's mechanism has the cathode and oxidant reaction consuming electrons, leaving hole generation at the exposed SiC. This somewhat agrees with the experimental data in this thesis, especially those with higher electrolyte concentration in Figure 12. That said, control experiments demonstrate that some Pt is needed for the etch to happen.

All MacEtch processes require an electrolyte. Bohn et al. proposed a theory implying that etching would be possible, given enough hole generation (assuming that holes are generated by UV light, from 1), without any oxidant other than H_2O. That is not experimentally demonstrated. It is possible that it is correct for the Si face of the crystal but almost certainly not for the C face of the crystal, given its unique oxidation properties[44,47].

It is possible that α-SiC (4H and 6H) etches porously as does pure Si in anodic etching. Figure 14 displays the current dependence of Si etched anodically, with I_{PSL} indicating the regime in which a porous layer is formed, and I_{OSC} indicating when smooth etching is achieved. This is in agreement with results found herein and in literature, namely that more intense UV light, which would potentially increase the charge in the substrate past the equivalent I_{PSL}[48], the current associated with formation of a porous layer, would lead to nonporous etching.

Consider that under thermal oxidation the C-face of 4H SiC oxidizes to $Si_4C_4O_4$ and $Si_4C_{4-x}O_2$[44]. Given the significant difference in HF removal energy and similar formation energy of these

two oxides it is possible that these account for the porous layer. The two complex oxides form randomly across the etch surface but are not removed at the same rate, leaving a porous layer behind.

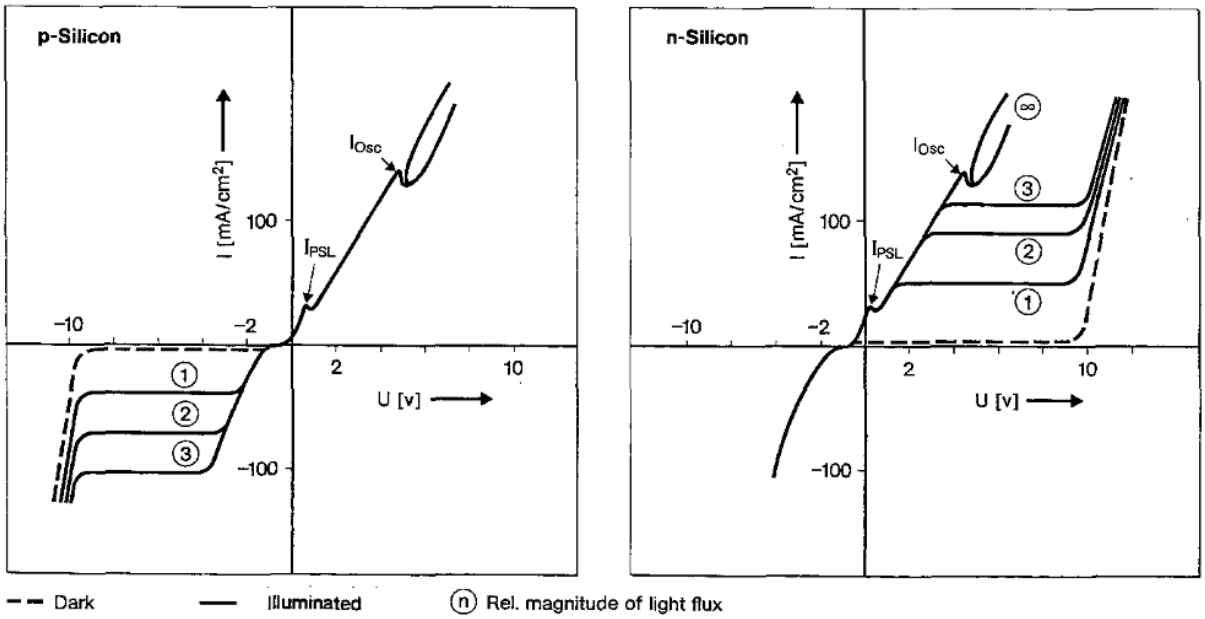

Figure 14: I-V characteristics of anodically etched SiC, measured during etching. $I < I_{PSL}$ corresponds to totally porous etching, $I_{PSL} < I < I_{OSC}$ corresponds to grainy etching, and $I_{OSC} < I$ corresponds to smooth etching[48].

If this is assumed to be the case, chemical reaction (4) needs only the addition that holes are also generated locally at SiC. That said, without Pt, the reaction does not work, so the dissociation must be key to the reaction, or something else is happening at the cathode that has not yet been considered. Reaction (5) needs a complex silicon carbon oxide in the products, for the C face[44,47]. It is likely that the Si face and C face have separate equations that describe their oxidation given their vastly different thermal oxidation behavior. Finally, reaction (6) needs to account for the removal of the new products ($Si_4C_4O_4$ and $Si_4C_{4-x}O_2$) of (2). Chemical reaction (7) corresponds to the reaction at the cathode (Pt), modified to agree with Leitgeb et al.[46]. Reaction (8) describes the oxidation behavior at the Si face, which is unchanged from the previously proposed

mechanism. Reactions (9) and (10) give the oxidation of the C face for the two possible complex silicon carbon oxides.

$$4S_2O_8^{2-} + 8e^- \rightarrow 8SO_4^{2-} \quad (7)$$

$$SiC + 4H_2O + 8h^+ \rightarrow SiO_2(s) + 8H^+ + CO_2(g) \quad (8)$$

$$4SiC + 2H_2O + 4h^+ \rightarrow Si_4C_4O_4(s) + 8H^+ \quad (9)$$

$$4SiC + (2 + 2x)H_2O + 4h^+ \rightarrow Si_4C_{4-x}O_2(s) + (4 + 4x)H^+ + xCO_2(g) \quad (10)$$

Reactions (11), (12) and (13) are the subsequent oxide removal processes that follow reactions (8), (9), and (10) respectively. Note that according to Dhar et al., removal reactions (9) and (10) require more energy and, given passivation or the slower reaction, are the first explanation of the porous layer in the MacEtch process.

$$SiO_2 + 6HF \rightarrow H_2SiF_6 + 2H_2O \quad (11)$$

$$Si_4C_4O_4 + 24HF + 4H_2O \rightarrow 4H_2SiF_6 + 4CO_2 + 24H^+ \quad (12)$$

$$Si_4C_{4-x}O_2 + 24HF + (6 - 2x)H_2O \rightarrow 4H_2SiF_6 + (4 - x)CO_2 + (28 - 4x)H^+ \quad (13)$$

Given that the removal and binding energies of these silicon carbon oxides are approximately 2.5 and 2.8 times higher than those of SiO_2[44], they are unevenly removed from the surface during etching in the locality of the more easily removed SiO_2. Density functional theory simulations of the removal of these oxides are shown in Figure 15, with the reaction schematic shown as well. Etching and oxidizing steps happen concurrently on the surface, so porous structures would be formed because of a dearth of local energy. Moreover, oxidation and removal of these different compounds would lead to additional inconsistencies in energy and thus produce even more variance in the etching. With a surplus of local energy this variance would shrink, leaving the surface smoother. The experimental evidence presented here agrees with this explanation; higher UV intensity tends to reduce porosity and moderate electrolyte concentrations

minimize porosity. Very high or low electrolyte concentrations promote porosity because they significantly lower overall local charge by either blocking UV with an increase in index of refraction or lacking carrier generation altogether, respectively.

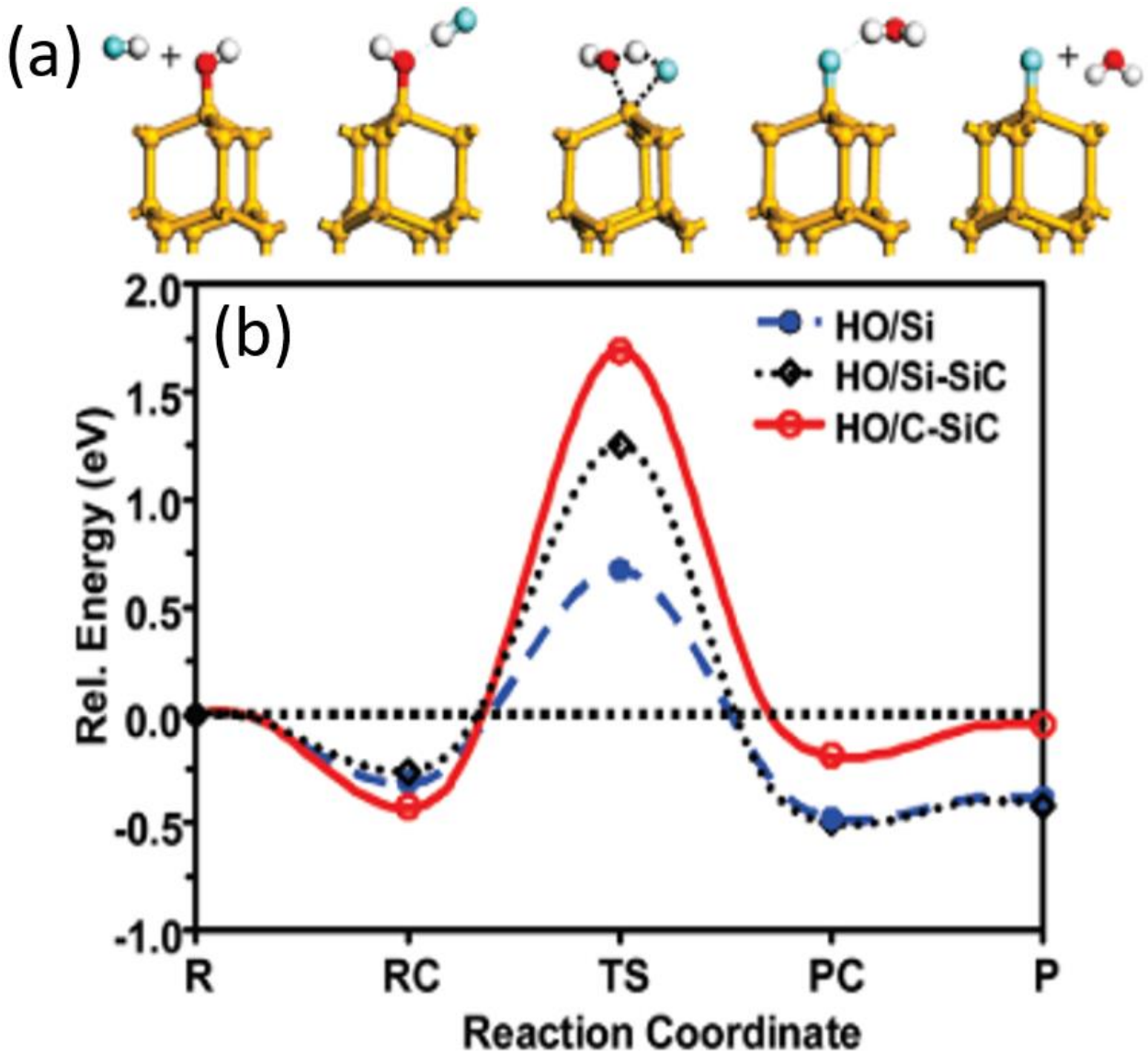

Figure 15: (a) Density function theory simulations of structures at each critical point involved during the removal of the –OH group by HF, forming SiF at the Si (111) surface. (b) Reaction energy plotted during the HF etch for oxidized Si(111), Si- and C- face SiC surfaces. R, RC, TS, PC, and P correspond to the stages of the reaction, those being reactants, reactant-complex, transition-state, product-complex, and products, respectively[44].

The second approach assumes that Leitgeb's chemical mechanism is correct and the structure of the etch is determined by the localized biasing, similar to the case in HF/Si etching as described by Föll[48]. Föll found that increased voltage bias significantly impacted the resulting etched surface in Si. Under low bias (corresponding to $I < I_{PSL}$, Figure 14) the resultant structure would be porous. The case is the same in the results presented for SiC with low UV power, either from high oxidant content, low UV power, or excessive etchant. At a moderate bias ($I > I_{PSL}$ in Figure 14) the etching would be grainy, inconsistent, but not porous; this mirrors the "nonporous" etching presented here. Föll's model would also predict that at high bias ($I > I_{osc}$ in Figure 14) that entirely smooth etching, regardless of orientation, would be observed.

The upshot of this analysis is that the current explanation in the literature is either incomplete or incorrect. The proposed mechanisms account for the porous nature of the etch, along with the mechanism to produce smoother etching. Keeping UV penetration (and therefore oxidant concentration and etchant depth) constant, the Pt cathode size and placement and mass transport would explain the etching rate and porosity dependence on pattern.

Further experiments are needed to determine which of these is correct (or perhaps, more correct). To test the first theory, a nuclear reaction analysis (NRA) of an etched sample would suffice. If in fact the silicon carbon oxides are formed (which will be confirmed by NRA), then this mechanism is correct. To test the second theory, a significantly stronger UV source would be needed to surpass the I_{osc} value (which is currently unknown) for smooth etching. It may be that both are correct, the second being a high-level view of the chemistry in the first. In that case, a fantastically precise mechanism will be obtained.

5. Conclusion

This thesis aimed to frame MacEtch as a promising research field that could replace the industry standard for nanoscale etching of SiC. Current etching methods were reviewed, with an emphasis on their ideal applications. Nonporous wet etching of SiC, a first, was presented in this thesis. Control over undercut, porosity, and etch rate was demonstrated across several samples. Correlations of electrolyte concentration and mask pattern with etch rate and porosity were explored, with conclusions drawn from each experiment. An analysis of the etching mechanism was presented with two possible explanations to complement the current theory.

Though the presented experiments show promise for nanoscale etching, they are not ideal for large area patterning due to their slow etch rate. Further work should include systematic studies that work to enhance etch tailoring for specific applications and overall increases in etch rate. This likely could be achieved with strong UV intensities, but would be best approached with by first confirming the mechanism, as discussed in Section 4.3. Better understanding the mechanism would aide in designing future experiments, especially those intended to optimize etch characteristics for specific applications. An analysis of crystal damage is also imperative to make the case for the application of MacEtch in nanoscale etching. Given that it is a wet etch, it is unlikely that it will produce any crystal damage or require any repair after etching.

Nanoscale devices, especially those based on intentional defects, need a precise etch that does not damage the crystal. For this reason, current dry etching techniques are not optimal for the fabrication of nanoscale devices. Therefore, due to its demonstrated precision, and the likelihood that it produces no crystal damage, MacEtch should be considered the premier method to etch nanoscale features in SiC.

References

[1] B. Bhushan, *Springer Handbook of Nanotechnology*, 4th ed. (Springer Verlag, Berlin, 2017).

[2] M. Mehregany, C.A. Zorman, N. Rajan, and C.H. Wu, Proc. IEEE **86**, 1594 (1998).

[3] H. Ou, Y. Ou, A. Argyraki, S. Schimmel, M. Kaiser, P. Wellmann, M.K. Linnarsson, V. Jokubavicius, J. Sun, R. Liljedahl, and M. Syvajarvi, Eur. Phys. J. B **87**, (2014).

[4] J.Y. Fan, X.L. Wu, and P.K. Chu, Prog. Mater. Sci. **51**, 983 (2006).

[5] A. Keffous, N. Gabouze, A. Cheriet, Y. Belkacem, and A. Boukezzata, Appl. Surf. Sci. **256**, 5629 (2010).

[6] J.R. Weber, W.F. Koehl, J.B. Varley, A. Janotti, B.B. Buckley, C.G. Van De Walle, and D.D. Awschalom, Proc. Natl. Acad. Sci. U. S. A. **107**, 8513 (2010).

[7] K. Szász, V. Ivády, I.A. Abrikosov, E. Janzén, M. Bockstedte, and A. Gali, Phys. Rev. B - Condens. Matter Mater. Phys. **91**, 1 (2015).

[8] M. Radulaski, M. Widmann, M. Niethammer, J.L. Zhang, S.Y. Lee, T. Rendler, K.G. Lagoudakis, N.T. Son, E. Janzén, T. Ohshima, J. Wrachtrup, and J. Vučković, Nano Lett. **17**, 1782 (2017).

[9] I.A. Khramtsov, A.A. Vyshnevyy, and D.Y. Fedyanin, Quantum Inf. **4**, (2018).

[10] J.B. Casady and R.W. Johnson, Solid. State. Electron. **39**, 1409 (1996).

[11] T.T. Mnatsakanov, L.I. Pomortseva, and S.N. Yurkov, Semiconductors **35**, 394 (2001).

[12] G.L. Harris, editor, *Properties of Silicon Carbide*, 1st ed. (INSPEC, Stevenage, 1995).

[13] J. Wang and X. Jiang, IET Power Electron. **13**, 445 (2020).

[14] V. Ivády, J. Davidsson, N.T. Son, T. Ohshima, I.A. Abrikosov, and A. Gali, Mater. Sci. Forum **924 MSF**, 895 (2018).

[15] A. Dräbenstedt, L. Fleury, C. Tietz, F. Jelezko, J. Wrachtrup, and A. Nizovtzev, Phys. Rev. B - Condens. Matter Mater. Phys. **60**, 11503 (1999).

[16] A. Gali, A. Gällström, N.T. Son, and E. Janzén, Mater. Sci. Forum **645**–**648**, 395 (2010).

[17] M. Radulaski, M. Widmann, M. Niethammer, J.L. Zhang, S.Y. Lee, T. Rendler, K.G. Lagoudakis, N.T. Son, E. Janzén, T. Ohshima, J. Wrachtrup, and J. Vučković, Nano Lett. **17**, 1782 (2017).

[18] J. Roy, S. Chandra, S. Das, and S. Maitra, Rev. Adv. Mater. Sci. **38**, 29 (2014).

[19] S. Tanaka, K. Rajanna, T. Abe, and M. Esashi, J. Vac. Sci. Technol. B Microelectron. Nanom. Struct. **19**, 2173 (2001).

[20] L.E. Luna, M.J. Tadjer, T.J. Anderson, E.A. Imhoff, K.D. Hobart, and F.J. Kub, J. Micromechanics Microengineering **27**, (2017).

[21] Q. Li, J.F. Wang, F.F. Yan, Z. Di Cheng, Z.H. Liu, K. Zhou, L.P. Guo, X. Zhou, W.P. Zhang, X.X. Wang, W. Huang, J.S. Xu, C.F. Li, and G.C. Guo, Nanoscale **11**, 20554 (2019).

[22] K.R. Williams, K. Gupta, and M. Wasilik, J. Microelectromechanical Syst. **12**, 761 (2003).

[23] R. Liu, H. Wu, H. Zhang, C. Li, L. Tian, L. Li, J. Li, J. Wu, and Y. Pan, J. Cryst. Growth **531**, 125351 (2020).

[24] D. Zhuang and J.H. Edgar, Mater. Sci. Eng. R Reports **48**, 1 (2005).

[25] S. Rysy, H. Sadowski, and R. Helbig, J. Solid State Electrochem. 437 (1999).

[26] S. Wang, Q. Huang, R. Guo, J. Xu, H. Lin, and J. Cao, Nanotechnology **31**, (2020).

[27] G. Károlyházy, D. Beke, D. Zalka, S. Lenk, O. Krafcsik, K. Kamarás, and Á. Gali, Nanomaterials **10**, 2 (2020).

[28] T.L. Rittenhouse, P.W. Bohn, T.K. Hossain, I. Adesida, J. Lindesay, and A. Marcus, J. Appl. Phys. **95**, 490 (2004).

[29] X. Li and P.W. Bonn, Appl. Phys. Lett. **77**, 2572 (2000).

[30] X. Li, Curr. Opin. Solid State Mater. Sci. **16**, 71 (2012).

[31] J.D. Kim, P.K. Mohseni, K. Balasundaram, S. Ranganathan, J. Pachamuthu, J.J. Coleman, and X. Li, Adv. Funct. Mater. **27**, 1 (2017).

[32] L. Li, C. Tuan, C. Zhang, Y. Chen, G. Lian, and C. Wong, J. Microelectromechanical Syst. **28**, 143 (2019).

[33] Z. Huang, N. Geyer, P. Werner, J. De Boor, and U. Gösele, Adv. Mater. **23**, 285 (2011).

[34] K. Balasundaram, P.K. Mohseni, Y.C. Shuai, D. Zhao, W. Zhou, and X. Li, Appl. Phys. Lett. **103**, (2013).

[35] P.K. Mohseni, S. Hyun Kim, X. Zhao, K. Balasundaram, J. Dong Kim, L. Pan, J.A. Rogers, J.J. Coleman, and X. Li, J. Appl. Phys. **114**, (2013).

[36] M. Dejarld, J.C. Shin, W. Chern, D. Chanda, K. Balasundaram, J.A. Rogers, and X. Li, Nano Lett. **11**, 5259 (2011).

[37] S.H. Kim, P.K. Mohseni, Y. Song, T. Ishihara, and X. Li, Nano Lett. **15**, 641 (2015).

[38] Y. Song, P.K. Mohseni, S.H. Kim, J.C. Shin, T. Ishihara, I. Adesida, and X. Li, IEEE Electron Device Lett. **37**, 970 (2016).

[39] H.C. Huang, M. Kim, X. Zhan, K. Chabak, J.D. Kim, A. Kvit, D. Liu, Z. Ma, J.M. Zuo, and X. Li, ACS Nano **13**, 8784 (2019).

[40] M. Leitgeb, C. Zellner, M. Schneider, and U. Schmid, ECS J. Solid State Sci. Technol. **5**, P556 (2016).

[41] Y. Chen, C. Zhang, L. Li, S. Zhou, X. Chen, J. Gao, N. Zhao, and C.P. Wong, Small **15**, 1 (2019).

[42] S.H. Kim, P.K. Mohseni, Y. Song, T. Ishihara, and X. Li, Nano Lett. **15**, 641 (2014).

[43] T.L. Rittenhouse, P.W. Bohn, and I. Adesida, Solid State Commun. **126**, 245 (2003).

[44] S. Dhar, O. Seitz, M.D. Halls, S. Choi, Y.J. Chabal, and L.C. Feldman, J. Am. Chem. Soc. **131**, 16808 (2009).

[45] J.C. Burton, L. Sun, and F.H. Long, Phys. Rev. B **59**, 7282 (1999).

[46] M. Leitgeb, C. Zellner, M. Schneider, S. Schwab, H. Hutter, and U. Schmid, J. Phys. D. Appl. Phys. **50**, (2017).

[47] I. Vickridge, J. Ganem, Y. Hoshino, and I. Trimaille, J. Phys. D. Appl. Phys. **40**, 6254 (2007).

[48] H. Föll, Appl. Phys. A Solids Surfaces **53**, 8 (1991).